STEM CELLS TRANSLATIONAL MEDICINE®

TISSUE ENGINEERING AND REGENERATIVE MEDICINE

Live Tissue Imaging to Elucidate Mechanical Modulation of Stem Cell Niche Quiescence

NICOLE Y.C. YU,[a] CONNOR A. O'BRIEN,[a] IVETA SLAPETOVA,[b] RENEE M. WHAN,[b] MELISSA L. KNOTHE TATE[a]

Key Words. Periosteum-derived stem cells • Stem cell niche quiescence • Tissue mechanical prestress • Confocal microscopy • In situ tissue imaging • Stem cell mechanics

[a]Graduate School of Biomedical Engineering and [b]Biomedical Imaging Facility, Mark Wainwright Analytical Centre, University of New South Wales, Sydney, New South Wales, Australia

Correspondence: Melissa L. Knothe Tate, Ph.D., Professor and Paul Trainor Chair of Biomedical Engineering, Graduate School of Biomedical Engineering, University of New South Wales, Samuels 509, Sydney 2052, New South Wales, Australia. e-mail: m.knothetate@unsw.edu.au

Received October 16, 2015; accepted for publication June 16, 2016; published Online First on July 28, 2016.

1066-5099/2016/$20.00/0

http://dx.doi.org/10.5966/sctm.2015-0306

ABSTRACT

The periosteum, a composite cellular connective tissue, bounds all nonarticular bone surfaces. Like Velcro, collagenous Sharpey's fibers anchor the periosteum in a prestressed state to the underlying bone. The periosteum provides a niche for mesenchymal stem cells. Periosteal lifting, as well as injury, causes cells residing in the periosteum (PDCs) to change from an immobile, quiescent state to a mobile, active state. The physical cues that activate PDCs to home to and heal injured areas remain a conundrum. An understanding of these cues is key to unlocking periosteum's remarkable regenerative power. We hypothesized that changes in periosteum's baseline stress state modulate the quiescence of its stem cell niche. We report, for the first time, a three-dimensional, high-resolution live tissue imaging protocol to observe and characterize ovine PDCs and their niche before and after release of the tissue's endogenous prestress. Loss of prestress results in abrupt shrinkage of the periosteal tissue. At the microscopic scale, loss of prestress results in significantly increased crimping of collagen of periosteum's fibrous layer and a threefold increase in the number of rounded nuclei in the cambium layer. Given the body of published data describing the relationships between stem cell and nucleus shape, structure and function, these observations are consistent with a role for mechanics in the modulation of periosteal niche quiescence. The quantitative characterization of periosteum as a stem cell niche represents a critical step for clinical translation of the periosteum and periosteum substitute-based implants for tissue defect healing. STEM CELLS TRANSLATIONAL MEDICINE *2017;6:285–292*

SIGNIFICANCE STATEMENT

Previous studies have shown a significant correlation of periosteum-derived stem cell tissue genesis with mechanical cues imbued through subtle physiological loading such as stance shift after surgery. How a change in baseline mechanical stress state can possibly be transduced to mesenchymal stem cells residing in the periosteal niche is a major conundrum in the field. A novel platform to integrate cutting-edge live cell and tissue imaging technology with the current understanding of stem cell-mediated tissue genesis and healing is described. The loss of baseline prestress intrinsic to periosteal tissue in a healthy, normal state results in an immediate and persistent shrinkage of tissue at a macroscopic scale that correlates with changes in collagen crimping and the number of rounded cell nuclei in the cambium layer of the tissue. Given a body of work demonstrating the link between stem cell and nucleus shape and lineage commitment, these results are consistent with a direct transduction of mechanical signals from a tissue to cellular length scale. These insights could have profound implications for mechanical regulation of periosteal stem cell niche quiescence.

INTRODUCTION

The periosteum, a composite cellular and connective tissue, bounds all nonarticular bone surfaces and provides a niche for mesenchymal stem cells (MSCs) [1–3]. Hyperelastic periosteal tissue exhibits a remarkable regenerative capacity; in critical size long bone defects surrounded in situ by periosteum, periosteum-derived cells (PDCs) egress from the tissue sheath within days of injury to regenerate tissue, infilling the defect with intramembranous woven bone within weeks [4] or endochondrally produced bone within months [5–8]. This process is modulated by both PDCs and periosteum's endogenous extracellular matrix (ECM) proteins [5, 6]. Mechanical loading has been shown to correlate with an increase in periosteum's tissue regeneration capacity [9, 10]. Mechanobiology has been hypothesized to be a key modulator of periosteal stem cell niche

quiescence; hence, an understanding of the mechanobiology of the periosteal niche is expected to facilitate use of the tissue and its resident cells in a translational context [7, 10–13].

Cells isolated from human periosteal tissue, referred to as periosteum-derived cells (PDCs), exhibit MSC surface markers, including CD73, CD90, and CD105 [3, 12]. Additionally, human PDCs express both epithelial and mesenchymal junctional adhesion proteins, providing a template for tissue architecture and playing a role in molecular mechanisms of chondro-, osteo-, and adipogenesis [8]. Although more PDCs reside in the inner cambium layer of the periosteum compared with the fibrous layer [1, 2, 7, 8, 14–17], greater than 99% of PDCs isolated through enzymatic digestion (encompassing cells from the fibrous and cambium layers both) and/or migration protocols (preferentially cells migrating from the cambium layer) exhibit MSC surface markers, including CD73, CD90, and CD105. In contrast, slightly less but more than 95%, 97%, and 95% of bone marrow stromal cells from human patients exhibit the MSC surface markers CD73, CD90, and CD105, respectively [3].

Periosteum and periosteum-inspired surgical membrane implants have been used to heal critical size bone [3, 5, 9, 10, 13, 18] and cartilage defects [19–23] in preclinical animal models and clinical (human) cases [24–29]. Numerous small animal studies have demonstrated the importance of the periosteum for bone healing [29, 30]. Removal of the periosteum has been shown to significantly reduce bone healing [30–33], and murine cell tracing experiments demonstrated that up to 90% of intramembranous and endochondral bone defect healing is derived from the periosteum [29]. A series of ovine studies demonstrated that retention of the periosteum in situ around a hematoma-filled defect is not only sufficient but also efficient for healing critical size femoral defects [5, 9, 10, 13, 18]. In vitro, progenitor cells from human periosteum exhibit the capacity for chondro-, osteo-, or adipogenesis, similar to or exceeding that of human bone marrow stromal cells. In these studies, cells were isolated either through trypsinization or by collection after egression from the cambium side of the sample [2, 3].

A key to translating periosteum's regenerative capacity is an understanding of the mechanical cues that trigger PDCs to egress and home to sites of injury. The outer fibrous layer of the periosteum is composed of the extracellular matrix structural proteins, collagen and elastin, which, respectively, impart toughness and elasticity to the tissue. Collagenous Sharpey's fibers anchor the periosteum to bone surfaces [1, 2, 7, 14–17]. Periosteum exhibits prestress in situ, comprising approximately 12.1 $\pm$ 0.40 MPa in the longitudinal direction and 0.77 $\pm$ 0.43 MPa in the circumferential direction of the adult ovine femur [7]. In parallel, periosteum exhibits anisotropic mechanical properties, with significantly higher elastic modulus in the longitudinal than in the circumferential direction. On separation of Sharpey's fibers due to periosteal lifting or resection, the stress state of the tissue changes abruptly, and the tissue shrinks anisotropically [33]. The subsequent rapid mobilization of periosteal MSCs to areas of injury and PDCs' genesis of repair tissue correlate significantly with the abrupt change in the periosteum's stress state [9, 4, 18]. Mechanical loading has also been shown to correlate with the altered patterns of gene expression associated with increased PDC proliferation [34].

A body of work in stem cell mechanics has pointed increasingly to a role for biophysical cues in modulating stem cell shape and fate [35–39]. In the context of these studies of periosteal mechanobiology and regeneration, our working hypothesis was that changes in the periosteum's baseline stress state would modulate the quiescence of its stem cell niche by altering the fate of the inhabitant PDCs. Our approach was to develop a live three-dimensional (3D) cell and tissue imaging protocol to study periosteal tissue and its inhabitant cell population and the changes in the same associated with the loss of tissue prestress. We hypothesized that the loss of prestress would result in changes to both periosteum's fibrous tissue architecture and its inhabitant PDC population.

Materials and Methods

Live cell and tissue imaging studies were performed to observe microscopic changes related to the loss of prestress in an ovine model. The rationale for the choice of the ovine model was twofold. First, we aimed to build on our previous body of work using the ovine model and its translation from in vitro [3, 33, 40] to ex vivo [10] to in vivo [4–6, 11, 13, 18] to clinical studies [3, 24, 25]. Also, in contrast to the few cell layer-thick murine periosteum [29], the ovine femoral periosteal thickness approximates that of humans [7, 17]. Specifically, measures of the ovine femur periosteum (i.e., 160.0 $\pm$ 23 μm [7, 17, 39, 40]) are similar to those of the human femoral periosteum thickness (i.e., 100 μm in patient donors aged 68–99 years) [2, 3, 17]. The periosteum thickness decreases significantly with age and sample site. For example, the mean thickness of the ovine tibial periosteum is approximately 417 μm at 2 years of age and 371 μm at 3 years of age. The mean thickness of the femoral periosteum in the older cohort is significantly smaller than that of the tibia from the same cohort [7].

Two-photon confocal microscopy was used for live and direct three-dimensional visualization of the cells and collagen structure within the periosteum. A cell-permeant fluorescent probe was selected to mark nucleic acids within the nucleus (DNA) and thereby identify cell nuclei instead of entire cells, facilitating identification of individual cells and easing cell count quantification. Two-photon confocal microscopy with second harmonics generation was used for collagen imaging without the need for freezing, cutting, or other techniques that could change the collagen structure of the tissue.

Periosteum Sample Harvest

Periosteum samples were harvested from the femora of male wether (castrated) sheep (n = 3). The sheep were harvested under the authority of the University of New South Wales Australia Animal Ethics Committee. Periosteal samples were resected and prepared for study following a modified, previously published protocol [40]. In brief, the skin and overlying muscle were removed to expose the femur under sterile conditions (Fig. 1A). The periosteum was carefully cleaned of muscle and tendon insertions using tweezers and a no. 10 surgical blade (Cincinnati Surgical Co., Cincinnati, OH, http://www.cincinnatisurgical.com). The femur and bounding periosteum were regularly saturated with Hartmann's solution (Baxter, Deerfield, IL, http://www.baxter.com) to retain moisture. Tissues (Fig. 1B) were isolated from the femur's medial and lateral aspect of the anterior diaphysis. To maintain in situ prestress (prestress group), samples were affixed to an annular, flexible plastic template (inner diameter, 10 mm; outer diameter, 20 mm; model no. PP2500; 3M, Maplewood, MN, http://www.3m.com) using ethyl 2-cyanoacrylate

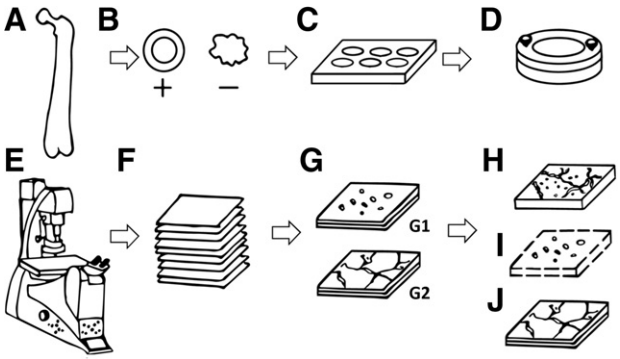

Figure 1. Methodology flowchart for elucidating the periosteal stem cell niche using confocal live cell imaging. **(A):** Isolation of ovine femur. **(B):** Resection of periosteum samples with prestress (+) or no prestress (−). **(C):** Sample tissue culture and fluorescent staining. **(D):** Placement of sample in chamber. **(E):** Live cell and tissue confocal imaging. **(F):** Collection of image stacks. **(G):** Image processing of separate image channels (cell nuclei **[G1]** and collagen **[G2]**). **(H):** Three-dimensional (3D) reconstruction of merged image stacks. **(I):** 3D cell counting. **(J):** Reconstruction of collagen with 3D image stacks.

glue (Loctite 435, medical grade; Henkel Australia, Kilsyth, VC, Australia, http://www.henkel.com.au) in accordance with previous protocols [40]. This allowed for tissue removal while maintaining in situ tissue length, width, and prestress state. A surgical blade was then used to cut along the outer edge of the plastic template, and periosteal elevators (model nos. 399.360 and 399.370; DePuy Synthes, West Chester, PA, http://www.synthes.com) were used to gently separate the Sharpey fibers from the underlying bone and resection of the periosteum. In the periosteum with no prestress (no prestress group), the circular plastic template was used as a guide, and sample resection followed the protocol for the prestress group, with the exception that the samples were allowed to shrink freely. A total of 8 samples were harvested per femur (i.e., n = 4 per group per sheep; Table 1).

Periosteum Sample Tissue Culture and Fluorescent Staining

Freshly isolated periosteum samples were directly transferred to tissue culture conditions in a humidified incubator at 37°C with 5% CO_2 in accordance with previously published protocols [3, 5]. The samples were stained fluorescently at set time points, either immediately after harvest or 3 days after harvest (Fig. 1C). In brief, the resected samples were transferred to 12-well tissue culture plates (CELLSTAR; Greiner Bio-One GmbH, Frickenhausen, Germany, http://www.greinerbioone.com) with the periosteum sample's cambium facing down. Each tissue culture well contained 2 ml of α-minimum essential medium (α-MEM) with GlutaMAX supplemented with 10% fetal bovine serum (FBS) (Thermo Fisher Scientific Life Sciences, Waltham, MA, http://www.thermofisher.com), 1% antibiotic-antimycotic (Thermo Fisher) overnight. Media were then changed to 2 ml of standard culture medium (α-MEM with GlutaMAX supplemented with 10% FBS, 1% penicillin-streptomycin; Thermo Fisher). The standard culture medium was replaced every 2–3 days.

The samples were imaged at two set time points (D_0, immediately after harvest, and D_3, 3 days after harvest). Specifically, group 1 and 2 samples were imaged at D_0 and group 3 and 4 samples were imaged at D_3. At the set time point (D_0 or D_3), the tissue samples were stained with fluorescent Hoechst 33342, trihydrochloride, trihydrate, 0.5 μg/ml prepared in standard culture medium (Thermo Fisher), a cell-permeant nuclear counterstain that emits fluorescence when bound to double-stranded DNA [41]. The samples were incubated in 2.5 ml of fluorescent stain mixture solution for 1.5 hours in a humidified incubator (37°C with 5% CO_2), washed with standard culture medium (3 washes, 10 minutes per wash), and stored in standard culture medium until immediately before confocal imaging, at which point the samples were washed in PBS (3 washes, 10 minutes per wash).

Table 1. Experimental groups

Group	Prestress state	Imaging time point (days after harvest)	Periosteal samples per sheep[a] (n)
1	Prestress	0	4
2	No prestress	0	4
3	Prestress	3	4
4	No prestress	3	4

[a]Three fields of view captured per sample.

Live Tissue Confocal Imaging

Each freshly stained periosteal sample was placed in a dual flow chamber (Warner Instruments, Hamden, CT, http://www.warneronline.com) with the cambium layer facing down and held between two glass cover slips (15 mm in diameter) and two silicon gaskets (Warner Instruments; Fig. 1D). For the prestressed groups (groups 1 and 3), each periosteum sample and annular template was placed in a dual flow chamber. Confocal imaging (TCS SP5 II multiphoton confocal laser scanning microscope with an HC PL Fluotar 20 $\times$ 0.50 NA dry objective; Leica Microsystems, Buffalo Grove, IL, http://www.leicamicrosystems.com) and multiphoton imaging (Mai Tai DeepSee Ti:Sapphire laser, 840 nm; Spectra Physics, Mountain View, CA, http://www.spectra-physics.com) enabled imaging of cell nuclei. The signal from the fluorescent dye Hoechst 33342 was collected in reflected non-descanned detectors (NDDs) fitted with emission filters of 460/50 nm. In addition, collection of the forward propagating second harmonics generation signal capture was achieved using transmitted NDDs with a 420/20-nm bypass filter. This enabled imaging of collagen in the periosteum (Fig. 1E). Three-dimensional stacks were acquired from the periosteal cambium to fibrous layers at 1.97-μm intervals (Fig. 1F), with signals representing cell nuclei and collagen (Fig. 1G). A total of three fields of view (310 μm $\times$ 310 μm) were collected per sample.

Image Processing

Captured image stacks were viewed and processed with ImageJ2, version 1.49 (NIH, Bethesda, MD, http://www.imagej.nih.gov). Three-dimensional reconstructions were generated using the 3D Viewer plugin (ImageJ2; NIH) to view the cell nuclei in relation to the collagen fibrils within the periosteal tissue (Fig. 1H). To determine the change in the number of cells exhibiting nuclear rounding (with and without prestress), image stacks of the cambium layer containing rounded nuclei-stained cells were delineated manually by a blinded observer and processed to remove background noise (ImageJ2; NIH), resulting in a binarized stack of clearly delimited particles representing nuclei. The particles

were quantified using the BoneJ: Particle Analyzer plugin (NIH) [42] on binarized image stacks. The nuclei number was normalized to the tissue volume (i.e., number of rounded cellular nuclei in three dimensions divided by the cambium tissue volume [nuclei per μm^3]; Fig. 1I).

The structure of the collagen matrix with and without prestress was observed using the 3D Viewer plugin and as two-dimensional (2D) images through stacks (ImageJ2; NIH; Fig. 1J). The change in 2D extracellular matrix structure immediately after harvest (D_0) was quantified as the degree of crimp in collagen filaments C, which was previously defined by $C = (l_c - l_s)/l_s \times 100\%$ [43]. The curved length of the collagen fiber bundle (l_c) and the length of the straight line (l_s) connecting the ends of the measured fiber bundle [43] followed previously published definitions [43] and were measured in a semiautomated fashion using the NeuroJ plugin (ImageJ2; NIH; supplemental online Fig. 1). Crimp was measured in three volumes of interest (VOIs) for each periosteum sample. For each VOI, a minimum of 10 collagen fibers was analyzed.

Statistical Analysis

Statistical analysis was performed using Prism (GraphPad, La Jolla, CA, http://www.graphpad.com). Significance was defined as $p < .05$. Cell nucleus rounding data were analyzed using nonparametric statistical tests (Kruskal-Wallis) with post hoc Mann-Whitney U tests to compare the prestress and no prestress groups and the D_0 and D_3 time points.

Results

Spatiotemporal in situ imaging of cells in their periosteal niche allowed for tracking of cell population changes concomitant with the measurement of changes in the periosteum's biomechanical milieu. Specifically, the live, three-dimensional tissue imaging method facilitated spatiotemporal in situ imaging of cell populations in their periosteal niche (Fig. 2). Periosteum tissue with prestress or with no prestress were imaged immediately or 3 days after harvest. Rounded cell nuclei in the cambium layer were counted in three dimensions to track the changes in the numbers of cells per volume exhibiting rounded nuclei concomitant with the measurement of changes in the periosteal biomechanical milieu. Periosteum with no prestress showed threefold and twofold higher densities of rounded cells compared with the prestress control group at D_0 and D_3 ($p < .01$), respectively (Fig. 3). Furthermore, qualitative observations of changes in crimp length suggested structural changes in the collagen in association with changes to the periosteal prestress state (Fig. 4A, 4B) and with respect to the tissue's cambium and fibrous layers (Fig. 5) immediately after harvest (D_0). Furthermore, quantitative measurements and qualitative observations of the changes in crimp suggested structural changes in the collagen due to periosteal prestress state change in the tissue's fibrous layers. The release of in situ periosteal prestress (i.e., no prestress) increased the degree of collagen crimp by twofold compared with samples with prestress ($p < .01$; Fig. 6).

Discussion

Loss in prestress of the periosteum, a consequence of the disruption of periosteum's Sharpey's fibers, resulted in immediate relaxation of the tissue, which was observed macroscopically as shrinkage in the unstressed sample. Under the microscope, tissue relaxation coincided with a significant increase in the degree of collagen crimping within the tissue. These changes in the macro- and microscopic architecture of collagen within the fibrous layer corresponded with changes in the number of cells exhibiting rounded nuclei. The development of a protocol to image live cells in situ within the periosteal niche provides a basis from which to unravel the regulation of stem cell niche quiescence and the triggering of stem cell activation.

In the cambium layer, the number of cells exhibiting rounded nuclei increased immediately on removal of prestress from the periosteal tissue, before proliferation or migration of the cells could possibly occur. Hence, these changes are indicative of an immediate change in nuclear shape coinciding with relaxation of prestress in the tissue. The density of cells with rounded nuclei (number of cells per volume) increased by approximately threefold on relaxation of the tissue and persisted after 3 days in culture. Similarly, the number of rounded nuclei in samples with and without prestress did not change significantly from day 1 to day 3 in culture.

The nucleus is a cellular mechanosensor with lamins (A/C and B1/2) that contribute to nuclear-cytoskeletal coupling and mechanotransduction [44]. Recent studies have shown that

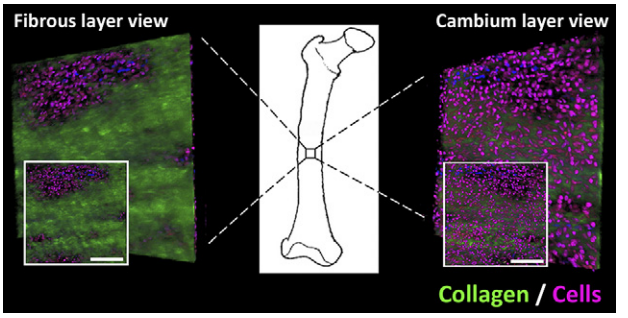

Figure 2. Representative three-dimensional live tissue image of the periosteal stem cell niche. Depicted three dimensionally from outer fibrous layer (left) and inner cambium layer (right), with two-dimensional views shown (insets). Collagen indicated by green and nuclei by blue and purple. Scale bars = 100 μm.

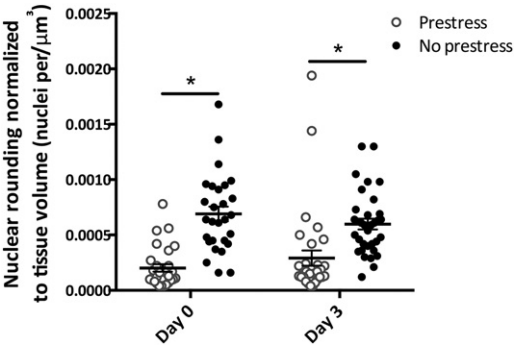

Figure 3. Number of rounded cell nuclei in the cambium of periosteum with and without prestress immediately after harvest (day 0) and 3 days after harvest (day 3), normalized to tissue volume (nuclei per μm^3). Line represents the median value of the group. $*$, $p < .01$ for comparison with prestress group. Error bars represent SEM.

Stem Cells Translational Medicine published by Wiley Periodicals, Inc. on behalf of AlphaMed Press

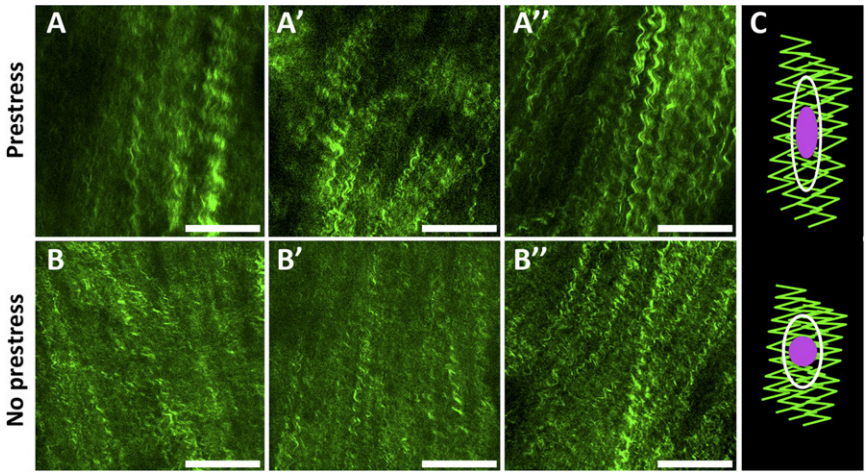

Figure 4. Representative images of collagen in periosteal fibrous layer immediately after harvest with prestress **(A, A′, A″)** and without prestress **(B, B′, B″)**, and schematic of working hypothesis **(C)**. The working hypothesis was that loss of intrinsic tissue prestress and concomitant relaxation in collagen crimping at fibrous layer would lead to cell nucleus shape change (rounding) at the cambium layer. Collagen is represented in green, cell nucleus in purple, and cell boundary in white. Scale bars = 100 μm.

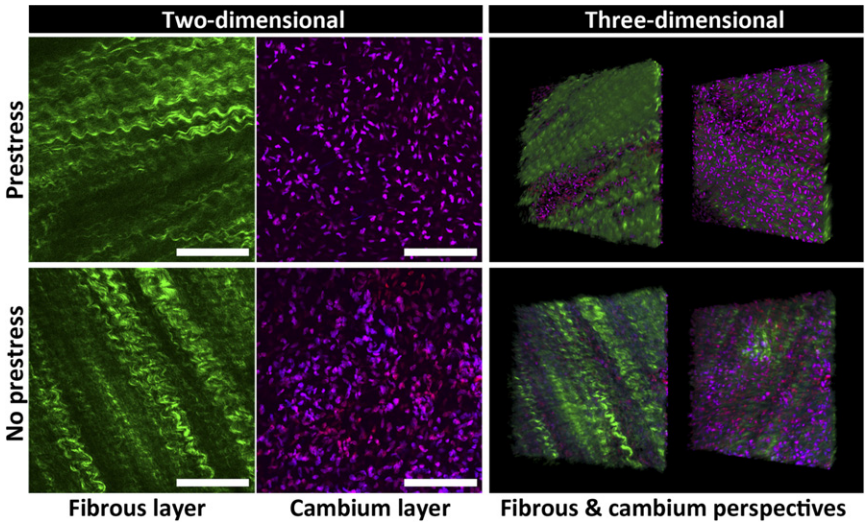

Figure 5. Projections representing the periosteal stem cell niche with prestress (top) and no prestress (bottom) in two and three dimensions. Cell nuclei (purple) and collagen (green) are shown from outer fibrous layer to inner cambium layer of the periosteum. Scale bars = 100 μm.

mechanotransduction mechanisms in the nucleus facilitate dynamic regulation of the nucleoskeleton in response to mechanical stress [45]. An increasing body of work on nuclear mechanotransduction has linked changes in nuclear shape and structure with physical forces [37, 38, 45–47]. Further studies have shown mechanical coupling between the extracellular matrix and the cell nucleus [37, 38, 46–49]. Mechanical stress stimuli can be transmitted through a direct molecular link between the extracellular molecules and the nucleoplasmic compartment [48]. Differences in stress transmission between the extracellular matrix and the nucleus also show cell type-dependent responses in nuclear structures [45].

As highlighted by cell migration studies, temporal nuclear shape changes can be viewed as a "negative image" of the physical space and discontinuities of the extracellular matrix [44]. Changes in nuclear shape and structure can lead to conformational changes in chromatin structure and organization that directly changes transcription regulation [37, 38, 46, 47]. Furthermore, nucleus shape and structure changes are also strongly related to modulation in cellular function and phenotype in both physiological and pathological situations, especially in a mechanically stimulated tissue environment [47]. For example, compression-induced shape changes in chondrocyte nuclei are associated with changes in cartilage composition and density [50, 51]. The shape and size of the nucleus is dependent on the cell type and can vary within cell lines; however, most cells imaged in situ and in 3D culture show ovoid or spherical nuclei with a diameter of 5–15 μm [44, 52]. In contrast, 2D culture leads to more spread out cells with disk-shaped nuclei with a diameter of 10–20 μm and a few microns in height [44, 52]. Because nuclear shapes and sizes can vary among extracellular matrix structures [44, 52, 53], our in situ 3D live tissue imaging protocol demonstrates greater physiological relevance compared with 2D culture models.

In the fibrous layer, the degree of collagen crimp increased with release of in situ prestress. Immediately after harvest, the

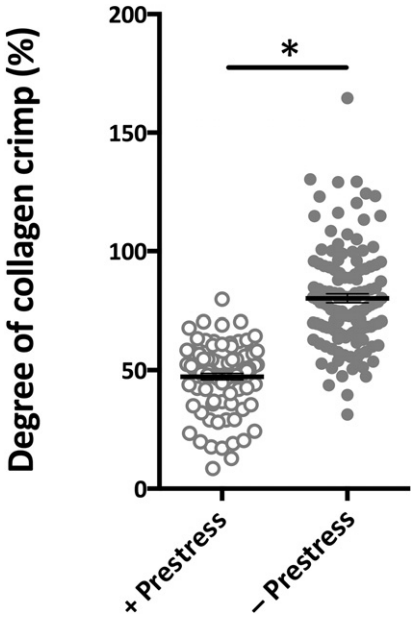

Figure 6. Degree of collagen crimp between samples with and without prestress immediately after harvest. In samples maintaining prestress, significantly less collagen crimp was observed than in samples without prestress. Line represents the median value of the group. *, $p < .01$ for comparison with prestress group. Error bars represent SEM.

degree of crimp increased by twofold. Previous studies have demonstrated significant tissue shrinkage after resection of periosteum without maintenance of prestress [7, 33]. The lack of tension on elastin fibers is expected to contribute to macroscopic tissue shrinking. A similar relationship between tension and collagen crimping is well-described for tendons [54–57], with tendon stretching decreasing the collagen crimp number and increasing the crimp angle (i.e., flattening) [54]. Our observation of a decrease in crimp length of collagen within the fibrous layer of the periosteum is consistent with these findings.

Our working hypothesis was that nuclear shape change (rounding) in the cambium layer would be related to loss of intrinsic tissue prestress and concomitant relaxation in collagen crimping in the fibrous layer (Fig. 4C). In addition, the observation of changes in collagen architecture in the present study suggests a role for collagen structure in the smart permeability properties of the periosteum. Thus, the permeability increases significantly when prestress is lost [40]. Finally, the observed abrupt change in nuclear shape might relate to changes in cell shape, structure, and function [35–39]. Such shape changes might provide a mechanism for the epithelial to mesenchymal transition observed with periosteal lifting and resection, in which PDCs stabilized by cell-cell junction proteins [8] become motile and egress into the hematoma-filled defect, rapidly proliferating and upregulating gene transcription for secretion of ECM proteins associated with tissue genesis [8, 35]. Taken as a whole and given the body of data tying stem cell and nucleus shape and fate [35–39], the rounding of nuclei in association with loss in periosteal prestress might trigger activation of PDCs residing in the cambium layer and loss of quiescence. Ongoing studies have been designed to elucidate the time course of these events.

Although our ultimate goal is to gain and apply these insights to harness the periosteum's regenerative capacity, fundamental studies are needed to understand cell behavior in a controlled yet physiological context. An inherent limitation of the present study was the use of resected ovine periosteum to understand the regulation of stem cell niche quiescence. The current model was designed to mimic conditions from our series of previous ovine studies demonstrating the regenerative potential of patent (intact vascular supply) and resected periosteum, in addition to PDCs isolated either through enzymatic digestion or egression of PDCs from resected periosteum [3–5, 13]. The inner cambium layer is composed of multiple cell types, with a significant subpopulation (>99%) of cambial cells identified as mesenchymal stem cells or periosteum-derived stem cells (PDCs) [3, 5]. Hence, the cambium layer can be seen as a putative MSC and osteochondral progenitor cell niche [1, 2, 7, 14–17]. In the present study, Hoechst nuclear stain was used to identify cells in the cambium layer. In addition, our current live imaging method is limited to population-based study of PDCs; however, future studies might enable single cell study of nuclear shape changes associated with loss in periosteal tissue's endogenous stress and changes in collagen crimping. To date, such single cell-based studies are limited to live cells in culture or fixed tissues; a shortcoming of studying fixed cells is the anisotropic shrinking of the extracellular matrix constituents and cells induced by chemical fixation [38].

A great impetus exists for elucidation of periosteum mechanobiology in the context of regenerative medicine [6, 11]. A number of in vivo preclinical studies have shown PDCs to be comparable or superior to bone marrow stem cells for bone healing and regeneration [3, 58–60]. In addition, recent studies of PDCs isolated from the periosteum of hip replacement patients have shown PDCs to have in vitro bone and cartilage generation capacity comparable to that of commercially available human bone marrow stromal cells [3]. PDCs isolated either by enzymatic digestion or migration exhibit subtle differences in the expression of surface markers typical for MSCs but no difference in proliferation or multipotency. Human PDCs have been better characterized than ovine PDCs, because the cell surface markers are commercially available for flow cytometry analysis, in addition to primers being widely available for the assessment of changes in gene transcription [2, 3, 61–65]. Hence, a limiting factor of our study was that, to date, the PDC surface markers available for human cells are not yet available for ovine cells. However, previous studies have demonstrated that ovine periosteal-derived cell morphological patterns of phenotype remain the same as those for human PDCs [2, 3]. Although we ultimately aim to translate the current approach to the human condition, access to sufficient quantities of fresh human periosteum with and without prestress is currently not ethically or practically feasible, although cutting edge imaging technologies enabling seamless imaging from the organ to the nano-length scale promise an exciting future in this regard [66, 67]. Quantitative characterization of ovine periosteum as a stem cell niche provides a critical step in the clinical translation of periosteum's regenerative power in the context of the ovine model and its recent application to limited human patients [25]. Important next steps include quantification of cell numbers and proliferation throughout the periosteal thickness, in both the cambium and the fibrous layers (e.g., through quantification of DNA). Also, as surface markers for cell cytometry and primers for quantitative polymerase chain reaction become available for ovine cells and tissues, it will be important to link our current understanding of human PDCs obtained during the course of hip replacement surgery [2, 3] to our understanding of periosteum

Stem Cells Translational Medicine published by Wiley Periodicals, Inc. on behalf of AlphaMed Press

modulated tissue generation in a well-established and controlled ovine femur segmental defect model [4, 5, 9, 10, 13, 18].

Conclusion

Using a novel live cell and tissue imaging protocol, we have demonstrated quantitatively that the loss of the periosteum's prestress coincides with a significant increase in nuclear rounding and changes in the architecture of ECM structural proteins of the stem cell niche. Taken together, these and previous studies provide a new appreciation for the role of mechanics in the modulation of periosteal stem cell niche quiescence.

Acknowledgments

We thank Dr. Michael Carnell for image-processing technical advice. This work was supported by the Paul Trainor Foundation.

Author Contributions

N.Y.C.Y.: conception and design, collection and/or assembly of data, data analysis and interpretation, manuscript writing, final approval of manuscript; C.A.O.: data analysis and interpretation; I.S.: conception and design, collection and/or assembly of data, final approval of manuscript; R.M.W.: conception and design, collection and/or assembly of data, final approval of manuscript; M.L.K.T.: conception and design, data analysis and interpretation, manuscript writing, final approval of manuscript.

Disclosure of Potential Conflicts of Interest

M.L.K.T. has uncompensated employment and intellectual property rights. The other authors indicated no potential conflicts of interest.

References

1 Colnot C, Zhang X, Knothe Tate ML. Current insights on the regenerative potential of the periosteum: Molecular, cellular, and endogenous engineering approaches. J Orthop Res 2012;30:1869–1878.

2 Chang H, Knothe Tate ML. Concise review: The periosteum: Tapping into a reservoir of clinically useful progenitor cells. Stem Cells Translational Medicine 2012;1:480–491.

3 Chang H, Docheva D, Knothe UR et al. Arthritic periosteal tissue from joint replacement surgery: A novel, autologous source of stem cells. Stem Cells Translational Medicine 2014;3:308–317.

4 Knothe Tate ML, Ritzman TF, Schneider E et al. Testing of a new one-stage bone-transport surgical procedure exploiting the periosteum for the repair of long-bone defects. J Bone Joint Surg Am 2007;89:307–316.

5 Knothe Tate ML, Chang H, Moore SR et al. Surgical membranes as directional delivery devices to generate tissue: Testing in an ovine critical sized defect model. PLoS One 2011;6:e28702.

6 Moore SR, Heu C, Yu NYC et al. Translating periosteum's regenerative power: Insights from quantitative analysis of tissue genesis within a periosteum substitute implant. Stem Cells Translational Medicine 2016;5:1–11.

7 Evans SF, Chang H, Knothe Tate ML. Elucidating multiscale periosteal mechanobiology: A key to unlocking the smart properties and regenerative capacity of the periosteum? Tissue Eng Part B Rev 2013;19:147–159.

8 Evans SF, Docheva D, Bernecker A et al. Solid-supported lipid bilayers to drive stem cell fate and tissue architecture using periosteum derived progenitor cells. Biomaterials 2013;34:1878–1887.

9 Knothe UR, Dolejs S, Matthew Miller R et al. Effects of mechanical loading patterns, bone graft, and proximity to periosteum on bone defect healing. J Biomech 2010;43:2728–2737.

10 McBride SH, Dolejs S, Brianza S et al. Net change in periosteal strain during stance shift loading after surgery correlates to rapid de novo bone generation in critically sized defects. Ann Biomed Eng 2011;39:1570–1581.

11 Knothe Tate ML, Yu NYC, Jalilian I et al. Periosteum mechanobiology and mechanistic insights for regenerative medicine. Bonekey Rep. (in press).

12 Caballero M, Reed CR, Madan G et al. Osteoinduction in umbilical cord- and palate periosteum-derived mesenchymal stem cells. Ann Plast Surg 2010;64:605–609.

13 Knothe Tate ML, Dolejs S, McBride SH et al. Multiscale mechanobiology of de novo bone generation, remodeling and adaptation of autograft in a common ovine femur model. J Mech Behav Biomed Mater 2011;4:829–840.

14 Squier CA, Ghoneim S, Kremenak CR. Ultrastructure of the periosteum from membrane bone. J Anat 1990;171:233–239.

15 Allen MR, Burr DB. Human femoral neck has less cellular periosteum, and more mineralized periosteum, than femoral diaphyseal bone. Bone 2005;36:311–316.

16 Allen MR, Hock JM, Burr DB. Periosteum: Biology, regulation, and response to osteoporosis therapies. Bone 2004;35:1003–1012.

17 Moore SR, Milz S, Knothe Tate ML. Periosteal thickness and cellularity in mid-diaphyseal cross-sections from human femora and tibiae of aged donors. J Anat 2014;224:142–149.

18 Knothe Tate ML, Dolejs S, Miller RM et al. Role of mechanical loading in healing of massive bone autografts. J Orthop Res 2010;28:1657–1664.

19 McCarthy HS, Roberts S. A histological comparison of the repair tissue formed when using either Chondrogide(®) or periosteum during autologous chondrocyte implantation. Osteoarthritis Cartilage 2013;21:2048–2057.

20 O'Driscoll SW. Articular cartilage regeneration using periosteum. Clin Orthop Relat Res 1999;(367, Suppl):S186–S203.

21 Harhaus L, Huang JJ, Kao SW et al. The vascularized periosteum flap as novel tissue engineering model for repair of cartilage defects. J Cell Mol Med 2015;19:1273–1283.

22 Gooding CR, Bartlett W, Bentley G et al. A prospective, randomised study comparing two techniques of autologous chondrocyte implantation for osteochondral defects in the knee: Periosteum covered versus type I/III collagen covered. Knee 2006;13:203–210.

23 Makris EA, Gomoll AH, Malizos KN et al. Repair and tissue engineering techniques for articular cartilage. Nat Rev Rheumatol 2015;11:21–34.

24 Knothe UR, Springfield DS. A novel surgical procedure for bridging of massive bone defects. World J Surg Oncol 2005;3:7.

25 Sauser B. Faster healing for severe fractures. MIT Tech Review March 10, 2010.

26 Gamal AY, Aziz M, Salama MH et al. Gingival crevicular fluid bone morphogenetic protein-2 release profile following the use of modified perforated membrane barriers in localized intrabony defects: A randomized clinical trial. J Int Acad Periodontol 2014;16:55–63.

27 Wakitani S, Mitsuoka T, Nakamura N et al. Autologous bone marrow stromal cell transplantation for repair of full-thickness articular cartilage defects in human patellae: Two case reports. Cell Transplant 2004;13:595–600.

28 Niedermann B, Boe S, Lauritzen J et al. Glued periosteal grafts in the knee. Acta Orthop Scand 1985;56:457–460.

29 Colnot C. Skeletal cell fate decisions within periosteum and bone marrow during bone regeneration. J Bone Miner Res 2009;24:274–282.

30 Ozaki A, Tsunoda M, Kinoshita S et al. Role of fracture hematoma and periosteum during fracture healing in rats: Interaction of fracture hematoma and the periosteum in the initial step of the healing process. J Orthop Sci 2000;5:64–70.

31 Zhang X, Xie C, Lin AS et al. Periosteal progenitor cell fate in segmental cortical bone graft transplantations: Implications for functional tissue engineering. J Bone Miner Res 2005;20:2124–2137.

32 Knothe Tate ML, O'Leary J, McNamara E et al. Lithotripsy stimulates new bone formation and mitigates loss of bone due to disuse in aged rats. Technol Health Care 2013;21:587–597.

33 McBride SH, Evans SF, Knothe Tate ML. Anisotropic mechanical properties of ovine femoral periosteum and the effects of cryopreservation. J Biomech 2011;44:1954–1959.

34 Raab-Cullen DM, Thiede MA, Petersen DN et al. Mechanical loading stimulates rapid changes in periosteal gene expression. Calcif Tissue Int 1994;55:473–478.

35 Knothe Tate ML, Falls TD, McBride SH et al. Mechanical modulation of osteochondroprogenitor cell fate. Int J Biochem Cell Biol 2008;40:2720–2738.

36 McBride SH, Knothe Tate ML. Modulation of stem cell shape and fate A: The role of density and seeding protocol on nucleus shape and gene expression. Tissue Eng Part A 2008;14:1561–1572.

37 McBride SH, Falls T, Knothe Tate ML. Modulation of stem cell shape and fate B: Mechanical modulation of cell shape and gene expression. Tissue Eng Part A 2008;14:1573–1580.

38 Zimmermann JA, Knothe Tate ML. Structure-function relationships in the stem cell's mechanical world A: Seeding protocols as a means to control shape and fate of live stem cells. Mol Cell Biomech 2011;8:275–296.

39 Chang H, Knothe Tate ML. Structure-function relationships in the stem cell's mechanical world B: Emergent anisotropy of the cytoskeleton correlates to volume and shape changing stress exposure. Mol Cell Biomech 2011;8:297–318.

40 Evans SF, Parent JB, Lasko CE et al. Periosteum, bone's "smart" bounding membrane, exhibits direction-dependent permeability. J Bone Miner Res 2013;28:608–617.

41 Lalande ME, Ling V, Miller RG. Hoechst 33342 dye uptake as a probe of membrane permeability changes in mammalian cells. Proc Natl Acad Sci USA 1981;78:363–367.

42 Doube M, Kłosowski MM, Arganda-Carreras I et al. BoneJ: Free and extensible bone image analysis in ImageJ. Bone 2010;47:1076–1079.

43 Rezakhaniha R, Agianniotis A, Schrauwen JT et al. Experimental investigation of collagen waviness and orientation in the arterial adventitia using confocal laser scanning microscopy. Biomech Model Mechanobiol 2012;11:461–473.

44 Friedl P, Wolf K, Lammerding J. Nuclear mechanics during cell migration. Curr Opin Cell Biol 2011;23:55–64.

45 Guilluy C, Burridge K. Nuclear mechanotransduction: Forcing the nucleus to respond. Nucleus 2015;6:19–22.

46 Roca-Cusachs P, Alcaraz J, Sunyer R et al. Micropatterning of single endothelial cell shape reveals a tight coupling between nuclear volume in G1 and proliferation. Biophys J 2008;94:4984–4995.

47 Dahl KN, Ribeiro AJ, Lammerding J. Nuclear shape, mechanics, and mechanotransduction. Circ Res 2008;102:1307–1318.

48 Martins RP, Finan JD, Guilak F et al. Mechanical regulation of nuclear structure and function. Annu Rev Biomed Eng 2012;14:431–455.

49 Wang N, Tytell JD, Ingber DE. Mechanotransduction at a distance: Mechanically coupling the extracellular matrix with the nucleus. Nat Rev Mol Cell Biol 2009;10:75–82.

50 Discher DE, Janmey P, Wang YL. Tissue cells feel and respond to the stiffness of their substrate. Science 2005;310:1139–1143.

51 Stewart CL, Roux KJ, Burke B. Blurring the boundary: The nuclear envelope extends its reach. Science 2007;318:1408–1412.

52 Jaalouk DE, Lammerding J. Mechanotransduction gone awry. Nat Rev Mol Cell Biol 2009;10:63–73.

53 Khatau SB, Hale CM, Stewart-Hutchinson PJ et al. A perinuclear actin cap regulates nuclear shape. Proc Natl Acad Sci USA 2009;106:19017–19022.

54 Franchi M, Fini M, Quaranta M et al. Crimp morphology in relaxed and stretched rat Achilles tendon. J Anat 2007;210:1–7.

55 Raspanti M, Manelli A, Franchi M et al. The 3D structure of crimps in the rat Achilles tendon. Matrix Biol 2005;24:503–507.

56 Diamant J, Keller A, Baer E et al. Collagen: Ultrastructure and its relation to mechanical properties as a function of ageing. Proc R Soc Lond B Biol Sci 1972;180:293–315.

57 Shah JS, Palacios E, Palacios L. Development of crimp morphology and cellular changes in chick tendons. Dev Biol 1982;94:499–504.

58 Agata H, Asahina I, Yamazaki Y et al. Effective bone engineering with periosteum-derived cells. J Dent Res 2007;86:79–83.

59 Hayashi O, Katsube Y, Hirose M et al. Comparison of osteogenic ability of rat mesenchymal stem cells from bone marrow, periosteum, and adipose tissue. Calcif Tissue Int 2008;82:238–247.

60 Ribeiro FV, Suaid FF, Ruiz KG et al. Periosteum-derived cells as an alternative to bone marrow cells for bone tissue engineering around dental implants: A histomorphometric study in beagle dogs. J Periodontol 2010;81:907–916.

61 Lim SM, Choi YS, Shin HC et al. Isolation of human periosteum-derived progenitor cells using immunophenotypes for chondrogenesis. Biotechnol Lett 2005;27:607–611.

62 Stich S, Loch A, Leinhase I et al. Human periosteum-derived progenitor cells express distinct chemokine receptors and migrate upon stimulation with CCL2, CCL25, CXCL8, CXCL12, and CXCL13. Eur J Cell Biol 2008;87:365–376.

63 Choi Y-S, Noh SE, Lim SM et al. Multipotency and growth characteristic of periosteum-derived progenitor cells for chondrogenic, osteogenic, and adipogenic differentiation. Biotechnol Lett 2008;30:593–601.

64 Ferretti C, Borsari V, Falconi M et al. Human periosteum-derived stem cells for tissue engineering applications: The role of VEGF. Stem Cell Rev 2012;8:882–890.

65 De Bari C, Dell'Accio F, Vanlauwe J et al. Mesenchymal multipotency of adult human periosteal cells demonstrated by single-cell lineage analysis. Arthritis Rheum 2006;54:1209–1221.

66 Knothe Tate ML, Zeidler D, Pereira AF et al. Organ-to-cell-scale health assessment using geographical information system approaches with multibeam electron microscopy. Adv Healthc Mater 2016;5:1581–1587.

67 Knothe Tate ML, Detamore M, Capadona JR et al. Engineering and commercialization of human-device interfaces, from bone to brain. Biomaterials 2016;95:35–46.

See www.StemCellsTM.com for supporting information available online.

Stem Cells Translational Medicine published by Wiley Periodicals, Inc. on behalf of AlphaMed Press